Brief Report

Characterization of kinase inhibitors targeting MAP tau hyperphosphorylation as potential therapeutic agents for Alzheimer's disease

Matilde Ercole[1], Jack A. Tuszynski[1,*]

[1] Department of Mechanical and Aerospace Engineering (DIMEAS) Politecnico di Torino, Corso Duca degli Abruzzi 24, Turin, I-10129, Italy

*Corresponding author: jacek.tuszynski@polito.it
DOI: To be assigned

Received 14 June 2026 Accepted 22 June 2026 Online published 30 June 2026

Abstract

Alzheimer's Disease (AD) is a progressive neurodegenerative disorder characterized by tau hyperphosphorylation, which contributes to neurofibrillary tangle formation and neuronal loss. Multiple kinases are involved in this process making them potential therapeutic targets. However, the identification of selective inhibitors with favourable pharmacokinetic properties and adequate brain penetration remains a challenge. In this study, thirteen tau-related kinases were prioritized according to the number of predicted tau serine phosphorylation sites identified using a percentile-based filtering approach. Known inhibitors for each kinase were evaluated using Boltz-2 AI-based docking software and predicted binding affinity likelihood (BAL) scores and IC_{50}-like values were combined to rank inhibitors within each kinase-specific set. The selected compounds were subsequently evaluated using SwissADME pharmacokinetic software, focusing on blood-brain barrier permeability, gastrointestinal absorption, P-glycoprotein interaction, and compliance with Lipinski's rule of five. Molecular selectivity was estimated using experimentally determined IC_{50} data retrieved from ChEMBL, while protein brain expression and protein–protein interaction data were obtained from the Human Protein Atlas and STRING databases. The results identified kinase inhibitors with favourable predicted pharmacokinetic properties and varying degrees of target selectivity. Together, these analyses provide a framework for prioritizing kinase inhibitors for further investigation and experimental validation in the context of future AD therapy development.

Keywords: Alzheimer's disease; MAP tau phosphorylation; protein kinases; kinase inhibitors; blood-brain barrier; computational drug discovery

1. Introduction

Alzheimer's disease (AD) is a progressive neurodegenerative disorder and the most common cause of dementia in adults. It represents a major global health challenge associated with population aging and it is characterized by progressive cognitive decline and widespread neuronal loss. The disease affects tens of millions of individuals worldwide (Gong & Iqbal, 2008). At the molecular level, AD is characterized by two neuropathological hallmarks: extracellular amyloid-β (Aβ) plaques and intracellular neurofibrillary tangles (NFTs) composed of hyperphosphorylated MAP tau protein (Martin et al., 2013). Notably, the distribution of NFTs correlates strongly with cognitive decline (Delacourte & Defossez, 1986). Under physiological conditions, MAP tau regulates microtubule stability, whereas abnormal phosphorylation reduces its affinity for microtubules, leading to its detachment and cytoskeletal destabilization. Detached MAP tau subsequently aggregates into paired helical filaments (PHFs), which assemble into NFTs (Delacourte & Defossez, 1986). MAP tau's phosphorylation is tightly regulated by a balance between kinases and phosphatases and disruption of this balance is considered a key driver of pathology (Martin et al., 2013). The addition of negatively charged phosphate groups (see **Fig. 1**) alters the protein's electrostatic properties and induces conformational changes that significantly reduce its affinity for microtubules (Rawat et al., 2022).

More than twenty kinases are known to phosphorylate MAP tau and are commonly classified into three major groups according to substrate specificity: proline-directed protein kinases (PDPKs), including GSK3β, CDK5, and MAPKs such as p38, ERK1/2, and JNK; non-proline-directed protein kinases, including TTBK1/2, DYRK1A, CK1/2, and members of the PKA, PKB, and PKC families; and tyrosine kinases,

Journal of Multiscale Neuroscience

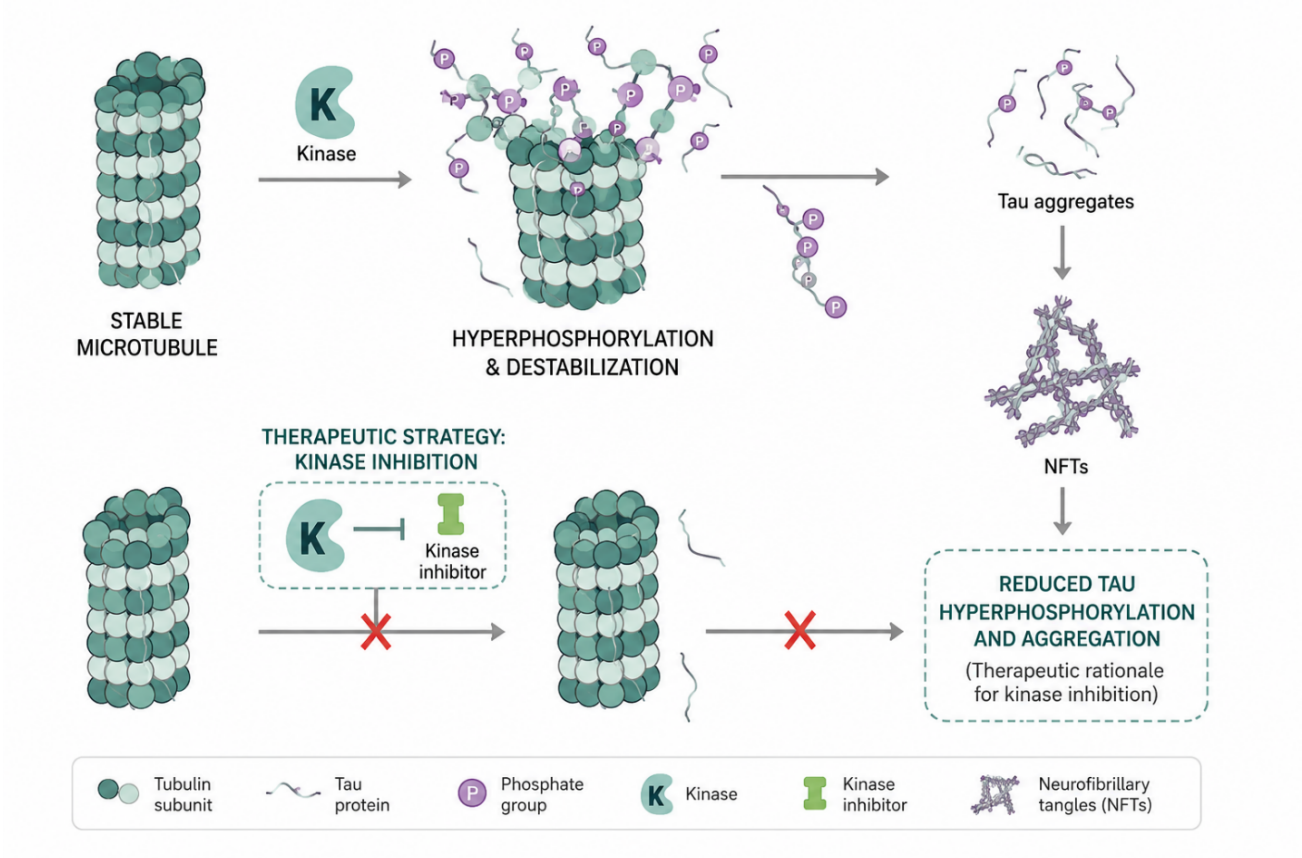

Figure 1 Schematic representation of MAP tau hyperphosphorylation and its contribution to microtubule destabilization, tau aggregation, and neurofibrillary tangle formation in Alzheimer's disease. Kinase inhibition is shown as a potential therapeutic strategy to reduce tau pathology.

including Src-family members such as Fyn, which are involved in MAP tau trafficking and synaptic function (Martin et al., 2013). Although tau-related kinases represent potential therapeutic targets, their involvement in multiple physiological signalling pathways complicates the development of selective inhibitors and increases the risk of off-target effects. In this study, a computational workflow was used to evaluate the binding profiles, selectivity, and pharmacokinetic properties of kinase inhibitors associated with tau phosphorylation, which is graphically illustrated in **Fig. 2**. The objective was to prioritize compounds for further investigation in the context of a future development of potential therapeutics for Alzheimer's disease.

2. Methods

2.1. Selection of tau kinases and structural data

Tau-phosphorylating kinases were selected based on literature evidence supporting their involvement in tau phosphorylation (Martin et al., 2013). For kinases with multiple isoforms, a single representative human isoform was selected to avoid redundancy. Experimentally determined human X-ray crystal structures were retrieved from the Protein Data Bank (PDB) (Berman et al., 2000). When more than one structure was available for a given kinase, the structure with the highest resolution was selected. The final set included thirteen tau-related kinases with available crystal structures suitable for subsequent computational analyses (**Table 1**).

2.2. Sequence-based ranking of tau kinases

Tau kinases were ranked based on the number of predicted tau serine phosphorylation sites identified using the PhosphoSitePlus kinase prediction tool. Only serine residues were considered, as serine residues represent the majority of reported tau phosphorylation sites (Martin et al., 2013). For each tau serine phosphorylation site, kinase-specific site percentile values were retrieved from the PhosphoSitePlus. Higher percentile values indicate stronger predicted kinase-substrate associations. To retain high-confidence predictions, only kinase-site pairs with percentile values above the 75th percentile threshold (70.810) were included in the analysis. Kinases were then ranked based on the number of retained tau serine phosphorylation sites.

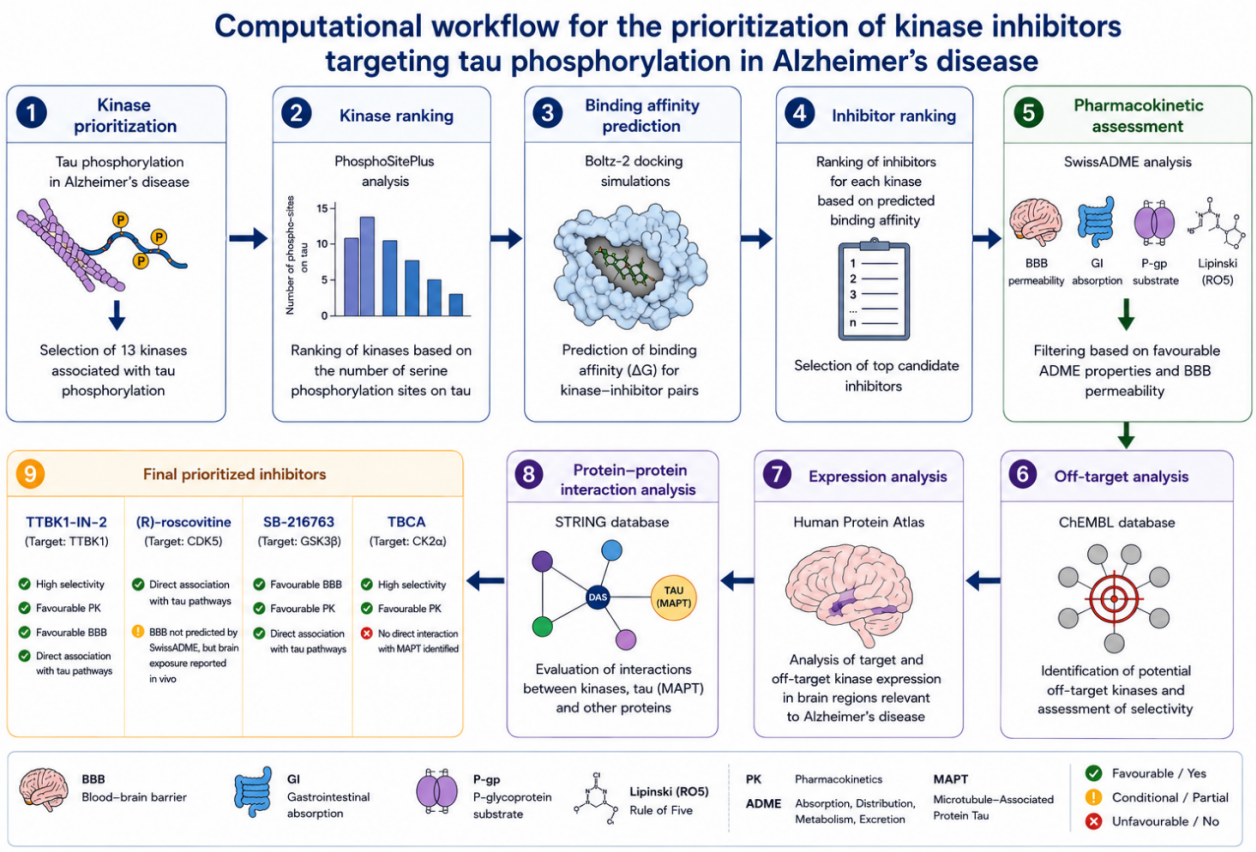

d

Figure 2 Overview of the computational workflow used to identify and prioritize kinase inhibitors targeting tau phosphorylation in Alzheimer's disease.

Table 1 List of selected tau-phosphorylating kinases and their experimentally determined X-ray crystal structures obtained from the Protein Data Bank.

Enzyme	Gene	PDB ID	Resolution (Å)
CaMKII-α	CAMK2A	6VZK	2,55
CDK5	CDK5	300G	1,95
CK1δ	CSNK1D	6RCG	1,40
CK2α	CSNK2A1	5OOI	1,99
DYRK1A	DYRK1A	7O7K	1,82
ERK2	MAPK1	6SLG	1,33
GSK3β	GSK3B	7B6F	2,05
JNK3	MAPK10	2O0U	2,10
p38α	MAPK14	4EWQ	2,10
PKAα	PRKACA	5IZJ	1,85
PKBβ	AKT2	3D0E	2
PKCα	PRKCA	8U37	2,48
TTBK1	TTBK1	7ZHQ	1,80

2.3. Binding affinity prediction using Boltz-2

A set of known inhibitors was selected for each kinase based on literature reports (AlNajjar et al., 2022; Alvez et al., 2025). When only a limited number of reference inhibitors were available, additional commercially available kinase inhibitors were included to expand the ligand set. The complete list of inhibitors with their respective SMILES representations is summarized in Supplementary Material (**Table S1**). Kinase–inhibitor interactions were evaluated using Boltz-2 (Passaro et al., 2025), which predicts the binding affinity from protein sequences and ligand molecular representations. Protein sequences were retrieved from UniProt (Ahmad et al., 2025), while inhibitor SMILES

representations were obtained from PubChem (Kim et al., 2025). For each kinase-inhibitor pair, Boltz-2 (Passaro et al., 2025) generated a binding affinity likelihood (BAL) score, indicating the predicted probability of ligand binding, together with a predicted IC_{50}-like affinity value expressed as log10(IC_{50}). Lower IC_{50}-like values indicate stronger predicted interactions.

To compare inhibitors within each kinase-specific set, BAL and IC_{50}-like values were integrated into a composite score adapted from a previously published approach (Passaro et al., 2025).

The normalized affinity component and the final composite score are defined in **Eq. (1)** and **Eq. (2)**, respectively.

$$I_{\text{norm}} = \max\left(\frac{IC_{50,\max} - IC_{50}}{IC_{50,\max} - IC_{50,\min}}, 0\right) \quad (1)$$

$$S = I_{\text{norm}} \times BAL \quad (2)$$

IC_{50}-like values were first normalized within each kinase inhibitor set and then combined with the corresponding BAL score. The resulting composite scores were used only to rank inhibitors targeting the same kinase and were not compared across different kinase targets. For each kinase, the inhibitor with the highest composite score was selected for subsequent analyses.

2.4. Pharmacokinetic property prediction using SwissADME

Top-ranked inhibitors for each kinase were evaluated using SwissADME (Daina et al., 2017), to predict pharmacokinetic and drug-likeness properties relevant to CNS applications. The analysis included gastrointestinal (GI) absorption, blood–brain barrier (BBB) permeability, P-glycoprotein (P-gp) substrate prediction, and compliance with Lipinski's rule of five. Since crossing of the BBB is a key consideration for CNS application of inhibitors in the context of AD treatment, alternative high-scoring inhibitors were considered when the top-ranked compound was predicted not to cross the BBB, if they had similar composite scores.

2.5. Off-target analysis

To include in our assessment of potential inhibitors their risk prediction in pre-clinical studies, we have carried out an analysis of their off-target interactions, which could lead to detrimental side effects. The off-target profiles of the selected inhibitors were evaluated using experimentally determined IC_{50} data retrieved from the ChEMBL database (Zdrazil et al., 2024). Searches were performed using inhibitor SMILES representations, with priority given to single-protein targets from Homo sapiens. When insufficient human single-protein data were available, protein family or protein complex data from Homo sapiens, Rattus norvegicus, or Gallus gallus were also included. Relevant off-target interactions were identified based on relative inhibitory potency. Proteins with experimentally determined IC_{50} values within approximately threefold of the corresponding on-target IC_{50} value were considered relevant off-targets.

2.6. Biological context analysis

Protein expression profiles of selected kinase targets and relevant off-target proteins were analysed using the Human Protein Atlas (HPA) database, with particular focus on brain expression in the cerebral cortex and hippocampus. Protein-protein interaction networks were generated using STRING (Szklarczyk et al., 2025) with a high-confidence interaction score threshold of 0.700. When no interactions were identified at this threshold, a medium-confidence threshold of 0.400 was applied. A maximum of five first-shell interaction partners was retained for each network. For kinases not available in STRING, interaction networks were generated using GeneMANIA (Warde-Farley et al., 2010).

3. Results

3.1. Ranking of tau kinases

MAP tau kinases were ranked according to the number of predicted tau serine phosphorylation sites retained after application of the 75th percentile cutoff (**Fig. 3**). The number of predicted phosphorylation sites varied between 5 and 15 for the selected kinases. PRKCA showed the highest number of predicted phosphorylation sites (15), followed by PRKACA, TTBK1, and CAMK2A (13 each), while CSNK2A1, DYRK1A, and MAPK10 had fewer predicted sites. The complete list of retained phosphorylation sites is provided in Supplementary Material (**Table S2**). Despite its established role in tau phosphorylation, GSK3β was associated with a relatively low number of predicted serine phosphorylation sites. This may reflect the dependence of GSK3β on priming phosphorylation events mediated by other kinases; this mechanism is not fully captured by the sequence-based prediction approach used in this study (Martin et al., 2013). Although this ranking was based on sequence predictions rather than experimentally validated interactions, it provided a useful framework for prioritizing kinases for further analysis.

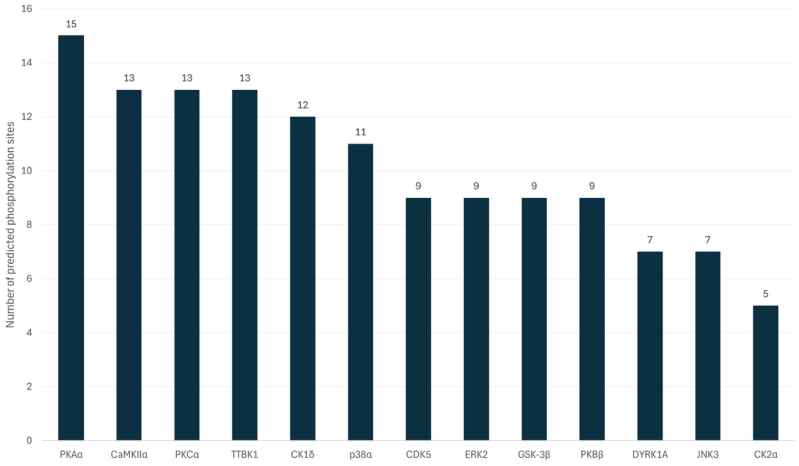

Figure 3 Number of predicted tau serine phosphorylation sites retained for each kinase after application of the 75th percentile cutoff.

3.2. Predicted binding affinity profiles

AI-based docking prediction software Boltz-2 (Passaro et al., 2025) was used to predict the interaction of each kinase–inhibitor pair. Predicted binding affinity likelihood (BAL) scores and IC_{50}-like values were combined into a single score (S), which was used to rank inhibitors within each kinase-specific set. The top-ranked inhibitor for each kinase was selected for further analysis (**Table 2**). Complete prediction outputs and composite scores are provided in Supplementary Material (**Table S3**). The IC_{50}-like values generated by Boltz-2 do not represent experimentally measured inhibitory potencies and should not be interpreted as absolute affinity estimates. Instead, IC_{50}-like values and BAL scores were used only for relative comparison among inhibitors evaluated under identical conditions. Consequently, identification of the top-ranked inhibitors reflects a comparative prioritization within each kinase rather than a direct prediction of in vivo efficacy. The selected inhibitors were subsequently evaluated for pharmacokinetic properties and off-target interactions.

3.3. Pharmacokinetic profile of selected inhibitors

Predicted pharmacokinetic properties were evaluated using SwissADME (Daina et al., 2017), with particular focus on blood–brain barrier (BBB) permeability, gastrointestinal absorption, P-glycoprotein (P-gp) substrate prediction, and compliance with Lipinski's rule of five (**Table 3**). When top-ranked inhibitors were predicted not to cross the BBB, alternative compounds with favourable BBB permeability and similar composite scores were evaluated. Following this approach, SB-216763, CCT128930, and SP600125 were selected instead of AR-A014418, Capivasertib, and AS601245 for GSK3β, PKBβ, and JNK3, respectively. For CDK5, none of the evaluated inhibitors showed favourable predicted BBB permeability. However, (R)-roscovitine was retained for further analysis due to previously reported in vivo brain exposure despite unfavourable SwissADME BBB predictions (Sallam et al., 2008). No alternative inhibitors for CaMKIIα, PKAα, p38α, and ERK2 combined favourable BBB permeability with binding scores comparable to those of the top-ranked compounds. These inhibitors were therefore retained despite their predicted limitations in CNS accessibility. Overall, the selected inhibitors showed favourable predicted pharmacokinetic properties, including high gastrointestinal absorption and compliance with Lipinski's rule of five. Most compounds were also predicted not to be P-gp substrates, supporting their potential use in CNS-related applications.

3.4. Off-target interaction profiles

Experimental IC_{50} data retrieved from ChEMBL showed clear differences in selectivity among the selected kinase inhibitors. Some compounds showed activity against multiple kinase targets, whereas others were more selective. The most relevant off-target interactions are summarized in **Table 4**. TTBK1-IN-2, TAK-715, and TBCA were the most selective inhibitors identified. In these three compounds, the IC_{50} values of the closest off-targets were substantially higher than those observed for the intended targets, indicating limited off-target activity based on the selectivity criteria used in this study. Several inhibitors showed limited selectivity among closely related kinase isoforms. IC261 inhibited CK1δ and CK1α with comparable potency, while FR-180204 displayed similar activity toward ERK2 and ERK1. Furthermore, SB-

Table 2 Top-ranked inhibitors identified for each kinase based on Boltz-2 binding affinity prediction and composite score ranking.

Kinase	Gene	Top-ranked inhibitor
PKCα	PRKCA	Go 6976
CaMKII-α	CAMK2A	KN93
PKAα	PRKACA	H-89
TTBK1	TTBK1	TTBK1-IN-2
CK1δ	CSNK1D	IC261
p38α	MAPK14	TAK 715
CDK5	CDK5	Olomoucine
ERK2	MAPK1	FR-180204
GSK3β	GSK3B	AR-A014418
PKBβ	AKT2	Capivasertib
DYRK1A	DYRK1A	DYRK1-IN-1
JNK3	MAPK10	AS601245
CK2α	CSNK2A1	TBCA

Table 3 Final selection of kinase inhibitors and their predicted pharmacokinetic properties, including gastrointestinal absorption, blood–brain barrier (BBB) permeability, P-glycoprotein substrate prediction, and compliance with Lipinski's rule of five.

Kinase	Inhibitor	GI - absorption	BBB permeant	P-gp substrate	Lipinski
PKCα	Go 6976	High	Yes	Yes	Yes; 0 violation
CaMKII-α	KN93	High	No	Yes	Yes; 1 violation: MW>500
PKAα	H-89	High	No	No	Yes; 0 violation
TTBK1	TTBK1-IN-2	High	Yes	No	Yes; 0 violation
CK1δ	IC261	High	Yes	No	Yes; 0 violation
p38α	TAK 715	High	No	Yes	Yes; 0 violation
CDK5	(R)-roscovitine	High	No*	Yes	Yes; 0 violation
ERK2	FR-180204	High	No	Yes	Yes; 0 violation
GSK3β	SB-216763	High	Yes	No	Yes; 0 violation
PKBβ	CCT128930	High	Yes	Yes	Yes; 0 violation
DYRK1A	DYRK1-IN-1	High	Yes	No	Yes; 0 violation
JNK3	SP600125	High	Yes	No	Yes; 0 violation
CK2α	TBCA	High	Yes	No	Yes; 1 violation: MLOGP>4.15

216763 and CCT128930 inhibited GSK3β/GSK3α and PKBβ/PKBα, respectively, with comparable potency. Go-6976 also displayed limited selectivity among classical PKC isoforms, inhibiting PKCα, PKCβ, and PKCγ at similar concentrations. In addition, FLT3 was identified as a relevant non-PKC off-target with potency comparable to that observed for PKCα. H-89, KN93, (R)-roscovitine, DYRK1-IN-1, and SP600125 showed the largest number of relevant off-target interactions. H-89 inhibited several kinases, including S6K1, AKT2, AKT3, and ROCK2, indicating limited target selectivity. KN93 showed comparable activity toward CaMKII and MLCK. (R)-Roscovitine inhibited multiple members of the CDK family, including CDK2, CDK5, CDK7, and CDK9, while DYRK1-IN-1 showed similar activity toward both DYRK and CLK family kinases. SP600125 exhibited the least selective profile, showing activity against JNK1, JNK2, FLT3, MPS1, and MELK in addition to its intended target JNK3. Together, these results suggest that the biological effects of these compounds may reflect the inhibition of multiple signaling pathways.

3.5. Expression profiles of selected targets and off-targets

Protein expression profiles of selected kinase targets and relevant off-targets were analysed using data from the Human Protein Atlas (HPA; https://www.proteinatlas.org.). Given the central role of the cerebral cortex and hippocampus in Alzheimer's disease pathology (Braak et al., 2006), protein expression in these brain regions was specifically eval-

Table 4 Summary of the most relevant off-target interactions identified for the selected kinase inhibitors. Off-targets were defined according to the IC_{50}-based selectivity criteria adopted in this study.

Inhibitor	Target	Most relevant Off-targets	Selectivity
Go 6976	PKCα	FLT3, PKCβ, PKC γ	Low
KN93	CaMKII-α	MLCK	Low
H-89	PKAα	S6K1, MSK1, AKT3, ROCK2, AKT2	Low
TTBK1-IN-2	TTBK1	-	High
IC261	CK1δ	CK1α	Moderate
TAK 715	p38α	-	High
(R)-roscovitine	CDK5	CDK2, CDK9, CDK1, CDK7	Low
FR-180204	ERK2	ERK1	Moderate
SB-216763	GSK3β	GSK3α, RPS6KB1	Moderate
CCT128930	PKBβ	PKBα	Moderate
DYRK1-IN-1	DYRK1A	CLK4, DYRK1B, CLK1, CLK2	Low
SP600125	JNK3	JNK1, JNK2, FLT3, MPS1, MELK	Low
TBCA	CK2α	-	High

uated. All primary kinase targets were detected in both the cerebral cortex and hippocampus, supporting their potential relevance to tau-related neuronal processes. CaMKIIα was the only target showing clear enrichment in these regions, whereas the remaining kinases were more uniformly expressed throughout the brain (**Fig. 4**). All analysed off-target kinases, except for MPS1 and MELK, were detected in both the cerebral cortex and hippocampus, indicating substantial overlap with the expression profiles of the primary targets. Several targets and off-targets were also annotated as predominantly expressed in neurons, suggesting overlap at both the regional and cellular levels. MPS1 and MELK were the only off-target kinases that were not detected in the cerebral cortex, hippocampus, or other examined brain regions according to HPA data. In contrast, their corresponding primary target, JNK3, was detected throughout the brain. This suggests that MPS1 and MELK may have a more limited role in CNS-related effects. The expression profiles of JNK3 and MPS1 are shown in (**Fig. 5**). Overall, a considerable overlap in brain expression was observed between the primary targets and most off-target kinases. This suggests that off-target interactions may contribute to the effects of several selected inhibitors.

3.6. Protein–protein interaction network analysis

Protein–protein interaction (PPI) networks were analyzed to examine the functional context of the selected kinase targets. The degree of network connectivity varied among kinases. CAMK2A, PRKACA, and CSNK1D formed highly connected networks with multiple interacting proteins, indicating their participation in broader signaling pathways (**Fig. 6**a–c). Among the analysed targets, CDK5 and GSK3B showed high-confidence interactions with MAPT, while TTBK1 displayed a direct interaction with MAPT at medium confidence (**Fig. 6**d–f). These results are consistent with the known role of these kinases in tau-related processes. Several interaction networks reflected relationships that were also observed in the selectivity analysis. For example, the MAPK1 network included MAPK3 (ERK1), while the AKT2 network included AKT1, consistent with the limited isoform selectivity observed for FR-180204 and CCT128930, respectively. In addition, GSK3β was connected to CSNK1A1, another kinase involved in tau phosphorylation, indicating that several tau-related kinases belong to interconnected signalling networks. Complete PPI networks for all analyzed kinases are provided in the Supplementary Material (**Fig. S1**). Overall, the network analysis highlighted both direct and indirect links between the selected kinase targets and tau-associated signalling pathways.

4. Conclusions

This study focused on finding suitable kinase inhibitors associated with MAP tau phosphorylation in Alzheimer's disease using a computational workflow that included kinase prioritization, binding affinity prediction, pharmacokinetic evaluation, and selectivity analysis. The results identified compounds with favourable predicted pharmacokinetic properties but also showed substantial differences in selectivity. Together, these findings indicate the importance of considering both CNS accessibility and target selectivity

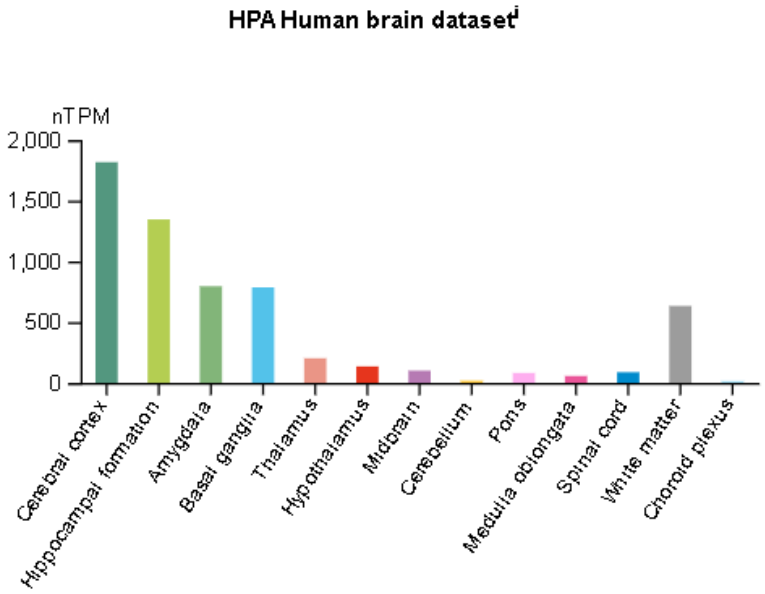

Figure 4 Regional brain expression profile of CaMKII-α according to Human Protein (https://www.proteinatlas.org) data. CaMKII-α shows enriched expression in cerebral cortex and hippocampal regions compared to other brain areas. Expression levels shown as normalized Transcripts Per Million (nTPM).

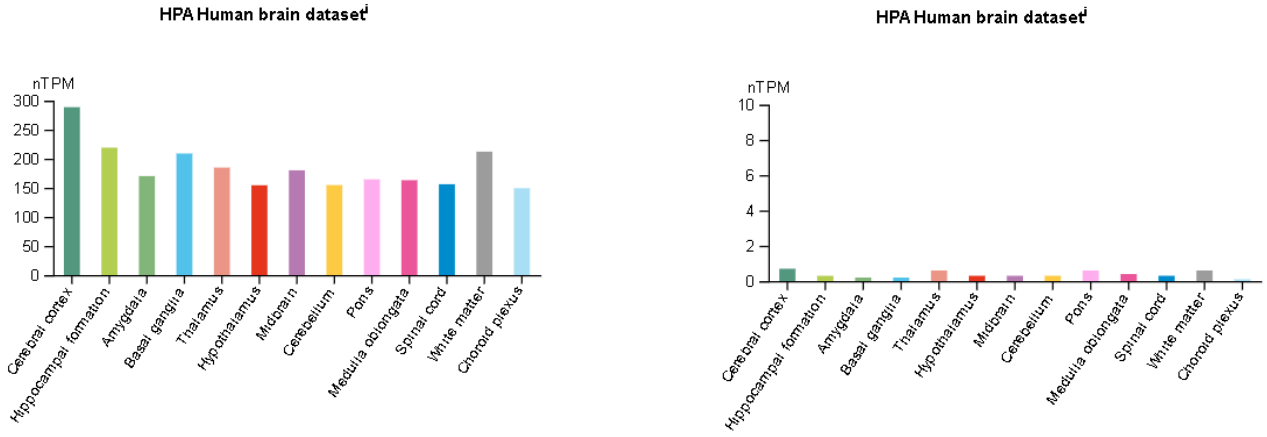

(a) **(b)**

Figure 5 Regional brain RNA expression profiles illustrating the different expression patterns of JNK3 and its off-target MPS1 according to Human Protein Atlas (https://www.proteinatlas.org) data. (a) JNK3 shows brain-enhanced expression. (b) MPS1 shows very low transcript levels across brain regions and is classified as not detected. Expression levels are shown as normalized Transcripts Per Million (nTPM)

during inhibitor prioritization. Among the selected compounds, TTBK1-IN-2 and TBCA showed the highest selectivity, whereas SB-216763 was selected because of its predicted blood–brain barrier permeability and activity against GSK3β, a kinase involved in tau phosphorylation. (R)-Roscovitine was retained for CDK5 despite its unfavourable BBB prediction, as previous in vivo studies have reported brain exposure. PPI analysis further showed a direct interaction between CDK5 and MAPT. Direct interactions with MAPT were also observed for GSK3β and TTBK1, supporting the involvement of these kinases in tau-related pathways. Overall, this study identified several promising kinase inhibitors with distinct pharmacokinetic and selectivity profiles and provides a basis for their further evaluation in future pre-clinical studies related to the development of therapeutic agents for Alzheimer's disease. Future work should focus not only on experimental validation of these predictions but also on the development of next generation compounds with improved selectivity and superior blood-brain-barrier penetration properties.

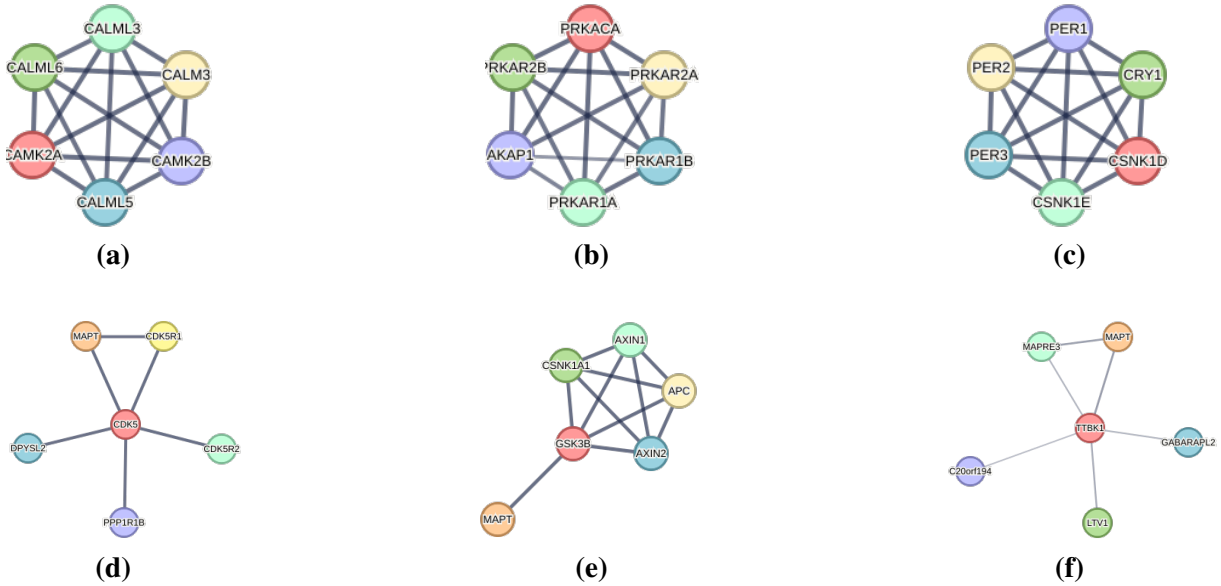

Figure 6 Protein–protein interaction networks of selected tau-related kinases obtained from STRING (Homo sapiens). Networks shown are CAMK2A (a), PRKACA (b), CSNK1D (c), CDK5 (d), GSK3B (e), and TTBK1 (f). CAMK2A, PRKACA, CSNK1D, CDK5, and GSK3B networks were generated using a high-confidence interaction threshold (interaction score ≥ 0.7), whereas the TTBK1 network was generated using a medium-confidence threshold (interaction score ≥ 0.4) to increase network connectivity.

References

Ahmad, S., da Costa Gonzales, L. J., Bowler-Barnett, E. H., Rice, D. L., Kim, M. et al. (2025) The uniprot website api: facilitating programmatic access to protein knowledge. *Nucleic Acids Research* **53**, W547–W553.

AlNajjar, Y. T., Gabr, M., ElHady, A. K., Salah, M., Wilms, G. et al. (2022) Discovery of novel 6-hydroxybenzothiazole urea derivatives as dual dyrk1a/alpha-synuclein aggregation inhibitors with neuroprotective effects. *European Journal of Medicinal Chemistry* **227**, 113911.

Alvez, M. B., Bergstrom, S., Kenrick, J., Johansson, E., Aberg, M. et al. (2025) A human pan-disease blood atlas of the circulating proteome. *Science* **390**, eadx2678.

Berman, H. M., Westbrook, J., Feng, Z., Gilliland, G., Bhat, T. N. et al. (2000) The protein data bank. *Nucleic Acids Research* **28**, 235–242.

Braak, H., Alafuzoff, I., Arzberger, T., Kretzschmar, H. & Del Tredici, K. (2006) Staging of alzheimer disease-associated neurofibrillary pathology using paraffin sections and immunocytochemistry. *Acta Neuropathologica* **112**, 389–404.

Daina, A., Michielin, O. & Zoete, V. (2017) Swissadme: a free web tool to evaluate pharmacokinetics, drug-likeness and medicinal chemistry friendliness of small molecules. *Scientific Reports* **7**, 42717.

Delacourte, A. & Defossez, A. (1986) Alzheimer's disease: Tau proteins, the promoting factors of microtubule assembly, are major components of paired helical filaments. *Journal of the Neurological Sciences* **76**, 173–186.

Gong, C.-X. & Iqbal, K. (2008) Hyperphosphorylation of microtubule-associated protein tau: a promising therapeutic target for alzheimer disease. *Current Medicinal Chemistry* **15**, 2321–2328.

Kim, S., Chen, J., Cheng, T., Gindulyte, A., He, J. et al. (2025) Pubchem 2025 update. *Nucleic Acids Research* **53**, D1516–D1525.

Martin, L., Latypova, X., Wilson, C. M., Magnaudeix, A., Perrin, M.-L. et al. (2013) Tau protein kinases: involvement in alzheimer's disease. *Ageing Research Reviews* **12**, 289–309.

Passaro, S., Corso, G., Wohlwend, J., Reveiz, M., Thaler, S. et al. (2025) Boltz-2: Towards accurate and efficient binding affinity prediction. bioRxiv preprint 2025.06.14.659707.

Rawat, P., Sehar, U., Bisht, J., Selman, A., Culberson, J. et al. (2022) Phosphorylated tau in alzheimer's disease and other tauopathies. *International Journal of Molecular Sciences* **23**, 12841.

Sallam, H., Jimenez, P., Song, H., Vita, M., Cedazo-Minguez, A. et al. (2008) Age-dependent pharmacokinetics and effect of roscovitine on cdk5 and erk1/2 in the rat brain. *Pharmacological Research* **58**, 32–37.

Szklarczyk, D., Nastou, K., Koutrouli, M., Kirsch, R., Mehryary, F. et al. (2025) The string database in 2025: protein networks with directionality of regulation. *Nucleic Acids Research* **53**, D730–D737.

Warde-Farley, D., Donaldson, S. L., Comes, O., Zuberi, K., Badrawi, R. et al. (2010) The genemania prediction server: biological network integration for gene prioritization and predicting gene function. *Nucleic Acids Research* **38**, W214–W220.

Zdrazil, B., Felix, E., Hunter, F., Manners, E. J., Blackshaw, J. et al. (2024) The chembl database in 2023: a drug discovery platform spanning multiple bioactivity data types and time periods. *Nucleic Acids Research* **52**, D1180–D1192.

Supplementary material

Table S1 A list of tau kinase inhibitors with their respoective SMILES representations

KINASE	INHIBITOR	SMILES
CaMKII-α	KN93	CN(C/C=C/C1=CC=C(C=C1)Cl)CC2=CC=CC=C2N(CCO)S(=O)(=O)C3=CC=C(C=C3)OC
	AIP	[H]N[C@@H](CCCCN)C(=O)N[C@@H](CCCCN)C(=O)N[C@@H](C)C(=O)N[C@@H](CC(C)C)C(=O)N[C@@H](CCCNC(N)=N)C(=O)N[C@@H](CCCNC(N)=N)C(=O)N[C@@H](CCC(N)=O)C(=O)N[C@@H](CCC(O)=O)C(=O)N[C@@H](C)C(=O)N[C@@H](C(C)C)C(=O)N[C@@H](CC(O)=O)C(=O)N[C@@H](C)C(=O)N[C@@H](CC(C)C)C(O)=O
CDK5	(R)-roscovitine	OC[C@H](NC1=NC(NCC2=CC=CC=C2)=C3C(N(C=N3)C(C)C)=N1)CC
	(R)-CR8	CC[C@@H](NC1=NC(NCC2=CC=C(C3=NC=CC=C3)C=C2)=C4N=CN(C(C)C)C4=N1)CO
	Olomoucine	CN1C=NC2=C(N=C(N=C21)NCCO)NCC3=CC=CC=C3
	Butyrolactone I	CC(=CCC1=C(C=CC(=C1)C[C@]2(C(=C(C(=O)O2)O)C3=CC=C(C=C3)O)C(=O)OC)O)C
	Purvalanols A	CC([C@@H](NC1=NC(NC2=CC=CC(Cl)=C2)=C3N=CN(C(C)C)C3=N1)CO)C
	Hymenialdisine	C\1CNC(=O)C2=C(/C1=C\3/C(=O)NC(=N3)N)C=C(N2)Br
CK1δ	IC261	COC1=CC(=C(C(=C1)OC)/C=C/2\C3=CC=CC=C3NC2=O)OC
	MU1742-amide-C6-acid	OC(CCCCCCC(N1CCC(F)(CC1)CN2C(C3=C4C(NC=C4)=NC=C3)=C(N=C2)C5=NC=C(C=C5)F)=O)=O
	SR-3029	FC1=CC(N2C=NC3=C(NCC4=NC5=CC=C(F)C(F)=C5N4)N=C(N6CCOCC6)N=C23)=CC=C1
	PF-5006739	NC1=NC=CC(C2=C(C3=CC=C(F)C=C3)N=CN2C4CCN(CC5=NOC=C5)CC4)=N1
CK2α	TBCA	C1=C(C(=C(C(=C1Br)Br)Br)Br)/C=C/C(=O)O
	Silmitasertib (CX-4945)	O=C(C1=CC=C2C3=C(C(NC4=CC=CC(Cl)=C4)=NC2=C1)C=CN=C3)O
	APL-5125 (Compound 61f)	O=C(O)C1=CC2=NC(OCCOCCCCNCC3=CC(F)=C(OC(F)(F)F)C(F)=C3)=C4C=CN=CC4=C2C=C1
	BioE-1115	O=C(C1=CC=C2N=C(C3=CC=C(F)C=C3)C(N(C)C(C)C)=NC2=C1)O
DYRK1A	Harmine	CC1=NC=CC2=C1NC3=C2C=CC(OC)=C3
	DYRK1-IN-1	CN(C)C1=NC(C2=C3C=CC=NN3N=C2)=CC=N1
	ZDWX-25	COC(=O)C1=CC2=C(C=C1)C3=C(N2)C(=NC=C3)NC(=O)C4CC4
	T3 CLK	O=C(NC=1N=C2C=CC(=CN2C1)C=3C=CN=CC3)C4=CC=C(C=C4)C(C(=O)N5CCN(C)CC5)(C)C
	INDY	O=C(C)/C=C1SC2=CC=C(O)C=C2N\1CC
	TC-S 7004	O=C(NC3=CC(C(NCC4=CC(Cl)=CC=C4)=O)=CC=C3Cl)C2=CC1=CN=C(OC)N=C1NC2=O
	TG 003	O=C(C)/C=C1SC2=CC=C(OC)C=C2N\1CC
ERK2	FR-180204	C1=CC=C(C=C1)C2=NN3C=CC=CC3=C2C4=CC5=C(NN=C5N=N4)N
	AZD0364	CC1=CN=C(N=C1C2=CN3CC(N(C(=O)C3=N2)CC4=CC(=C(C=C4)F)F)COC)NC5=CC=NN5C
	VX-11e	CC1=CN=C(N=C1C2=CNC(=C2)C(=O)NC(CO)C3=CC(=CC=C3)Cl)NC4=C(C=C(C=C4)F)Cl
	Ravoxertinib	CN1C(=CC=N1)NC2=NC=CC(=N2)C3=CC(=O)N(C=C3)C(CO)C4=CC(=C(C=C4)Cl)F
	Ulixertinib	CC(C)NC1=NC=C(C(=C1)C2=CNC(=C2)C(=O)NC(CO)C3=CC(=CC=C3)Cl)Cl
GSK3β	A 1070722	O=C(NC3=NC(C(F)(F)F)=CC=C3)NC2=CC=NC1=CC(OC)=CC=C12
	AZD 2858	O=C(NC=1C=NC=CC1)C=2N=C(C=NC2N)C3=CC=C(C=C3)S(=O)(=O)N4CCN(C)CC4
	6BIO	O/N=C(C1=CC=CC=C1N2)/C2=C3/C(NC4=C3C=CC(Br)=C4)=O
	CHIR 98014	NC1=NC(NCCNC2=NC=C(C(C3=C(C=C(C=C3)Cl)Cl)=N2)N4C=CN=C4)=CC=C1[N+]([O-])=O
	Kenpaullone	BrC1=CC=C2NC3=C(CC(=O)NC4=CC=CC=C34)C2=C1
	AR-A014418	COC1=CC=C(C=C1)CNC(=O)NC2=NC=C(S2)[N+](=O)[O-]
	SB-216763	CN1C=C(C2=CC=CC=C21)C3=C(C(=O)NC3=O)C4=C(C=C(C=C4)Cl)Cl
	SB-415286	C1=CC=C(C(=C1)C2=C(C(=O)NC2=O)NC3=CC(=C(C=C3)O)Cl)[N+](=O)[O-]
	ARN25068	C1CC1C2=CC(=NN2)NC3=NC(=NC4=C3SC=C4)NCC5=CC=CC=C5
	ZDWX-25	COC(=O)C1=CC2=C(C=C1)C3=C(N2)C(=NC=C3)NC(=O)C4CC4
	TC-G 24	CC(C=C3)=C(Cl)C=C3NC1=NN=C(C2=CC=C([N+]([O-])=O)C=C2)O1

Table S1 A list of tau kinase inhibitors with their respoective SMILES representations (continued.)

KINASE	INHIBITOR	SMILES
JNK3	SP600125	C1=CC=C2C(=C1)C3=NNC4=CC=CC(=C43)C2=O
	AS601245	C1=CC=C2C(=C1)N=C(S2)C(C#N)C3=NC(=NC=C3)NCCC4=CN=CC=C4
	JNK-IN-8	CC1=C(C=CC(=C1)NC(=O)C2=CC(=CC=C2)NC(=O)C=CCN(C)C)NC3=NC=CC(=N3)C4=CN=CC=C
	Tanzisertib HCl	C1CC(CCC1NC2=NC=C3C(=N2)N(C(=N3)NC4=C(C=C(C=C4F)F)F)C5CCOC5)O
	JNK inhibitor IX	C1CCC2=C(C1)C(=C(S2)NC(=O)C3=CC=CC4=CC=CC=C43)C#N
	Bentamapimod	C1COCCN1CC2=CC=C(C=C2)COC3=NC=CC(=N3)C(C#N)C4=NC5=CC=CC=C5S4
p38α	SB-239063	COC1=NC=CC(=N1)C2=C(N=CN2C3CCC(CC3)O)C4=CC=C(C=C4)F
	SB-203580	CS(=O)C1=CC=C(C=C1)C2=NC(=C(N2)C3=CC=NC=C3)C4=CC=C(C=C4)F
	BIRB-796	CC1=CC=C(C=C1)N2C(=CC(=N2)C(C)(C)C)NC(=O)NC3=CC=C(C4=CC=CC=C43)OCCN5CCOCC5
	SB 202190	OC1=CC=C(C=C1)C1=NC(=C(N1)C1=CC=NC=C1)C1=CC=C(F)C=C1
	SB 706504	N=C(NC#N)NCCNC1=NC(C4=C(C)C=C(F)C=C4)=C(C=CC(N2C3=C(F)C=CC=C3F)=O)C2=N1
	TAK 715	CCC1=NC(C3=CC(C)=CC=C3)=C(C2=C(NC(C4=CC=CC=C4)=O)N=CC=C2)S1
PKAα	H-89	C1=CC2=C(C=CN=C2)C(=C1)S(=O)(=O)NCCNC/C=C/C3=CC=C(C=C3)Br
	AT13148	C1=CC(=CC=C1C2=CNN=C2)C(CN)(C3=CC=C(C=C3)Cl)O
	KT 5720	O[C@@]1(C(OCCCCCC)=O)C[C@@H]2O[C@]1(N3C4=CC=CC=C4C5=C3C6=C(C7=C5CNC7=O)C8=CC=CC=C8N26)C
PKBβ	CCT128930	C1CN(CCC1(CC2=CC=C(C=C2)Cl)N)C3=NC=NC4=C3C=CN4
	Afuresertib (GSK2110183)	CN1C(=C(C=N1)Cl)C2=C(SC(=C2)C(=O)NC(CC3=CC(=CC=C3)F)CN)Cl
	Capivasertib (AZD5363)	C1CN(CCC1(C(=O)NC(CCO)C2=CC=C(C=C2)Cl)N)C3=NC=NC4=C3C=CN4
	GSK690693	CCN1C2=C(C(=NC=C2OCC3CCCNC3)C#CC(C)(C)O)N=C1C4=NON=C4N
	Miransertib (ARQ-092)	C1CC(C1)(C2=CC=C(C=C2)N3C4=C(C=CC(=N4)C5=CC=CC=C5)N=C3C6=C(N=CC=C6)N)N
	Ipatasertib (GDC-0068, RG7440)	CC1CC(C2=C1C(=NC=N2)N3CCN(CC3)C(=O)C(CNC(C)C)C4=CC=C(C=C4)Cl)O
PKCα	GF-109203X	CN(C)CCCN1C=C(C2=CC=CC=C21)C3=C(C(=O)NC3=O)C4=CNC5=CC=CC=C54
	Calphostin C	O=C1C(OC)=C(C[C@@H](C)OC(C2=CC=CC=C2)=O)C3=C4C5=C(C(OC)=CC(O)=C5C(C(OC)=C4C[C@@H](C)OC(OC6=CC=C(O)C=C6)=O)=O)C7=C(OC)C=C(O)C1=C73
	Go 6976	O=C(NC3)C1=C3C(C4=CC=CC=C4N5CCC#N)=C5C2=C1C6=C(C=CC=C6)N2C
	Go 6983	O=C(N1)C(C2=CNC3=C2C=CC=C3)=C(C4=CN(CCCN(C)C)C5=C4C=C(OC)C=C5)C1=O
TTBK1	TTBK1-IN-2	C1=CC(=CC=C1NC2=NC=NC3=C2C=CN3)OC4=CC=C(C=C4)Cl
	TTBK1-IN-1	O[C@@](C)(CC)C#CC1=CC2=C(C=CN2C3=CC(OC)=NC(N)=N3)C=N1

Table S2 A complete list of the retained phosphorylation sites on MAP tau with their corresponding kinases and genes encoding for them.

KINASE	GENE	PREDICTED MAPT SERINE PHOSPHORYLATION SITES
PKCα	PRKCA	S184-P;S191-P;S195-P;S208-P;S210-P;S214-P;S235-P;S237-P;S238-P;S241-P;S258-P;S305-P;S324-P;S352-P;S409-P
CaMKII-α	CAMK2A	S56-P;S113-P;S131-P;S184-P;S185-P;S191-P;S214-P;S237-P;S293-P;S320-P;S356-P;S409-P;S416-P
PKAα	PRKACA	S184-P;S185-P;S191-P;S210-P;S214-P;S237-P;S262-P;S293-P;S320-P;S324-P;S352-P;S356-P;S409-P
TTBK1	TTBK1	S195-P;S214-P;S238-P;S241-P;S258-P;S285-P;S316-P;S320-P;S341-P;S352-P;S412-P;S433-P;S435-P
CK1δ	CSNK1D	S56-P;S68-P;S113-P;S305-P;S324-P;S341-P;S352-P;S356-P;S412-P;S416-P;S433-P;S435-P

KINASE	GENE	PREDICTED MAPT SERINE PHOSPHORYLATION SITES
p38α	MAPK14	S46-P;S185-P;S191-P;S199-P;S202-P;S208-P;S235-P;S238-P;S396-P;S404-P;S422-P
CDK5	CDK5	S46-P;S191-P;S199-P;S202-P;S208-P;S235-P;S238-P;S396-P;S404-P;S422-P
ERK2	MAPK1	S46-P;S191-P;S199-P;S202-P;S235-P;S238-P;S396-P;S404-P;S422-P
GSK3β	GSK3B	S46-P;S113-P;S184-P;S199-P;S202-P;S208-P;S235-P;S305-P;S404-P
PKBβ	AKT2	S199-P;S214-P;S237-P;S262-P;S293-P;S320-P;S324-P;S352-P;S409-P
DYRK1A	DYRK1A	S46-P;S199-P;S202-P;S214-P;S235-P;S352-P;S404-P;S409-P
JNK3	MAPK10	S46-P; S199-P; S202-P; S235-P; S396-P; S404-P; S422-P
CK2α	CSNK2A1	S56-P; S113-P; S184-P; S341-P; S400-P

Table S3 A summary of the prediction outputs and composite scores for the top-ranked inhibitors of the MAP tau kinases.

KINASE	GENE	INHIBITORS	IC50-LIKE	BAL	SCORE
PKCα	PRKCA	GF-109203X	10.75	0.83	0.000
		Calphostin C	6.46	0.40	0.400
		Go6976	8.26	0.74	0.430
		Go6983	10.4	0.81	0.066
CaMKII-α	CAMK2A	KN93	9.54	0.09	0.090
		AIP	9.97	0.57	0.000
PKAα	PRKACA	H-89	8.62	0.75	0.750
		AT13148	10.87	0.92	0.000
		KT 5720	9.96	0.77	0.311
TTBK1	TTBK1	TTBK1-IN-2	7.05	0.37	0.370
		TTBK1-IN-1	7.24	0.14	0.000
CK1δ	CSNK1D	IC261	7.45	0.45	0.450
		MU1742-amide-C6-acid	10.64	0.96	0.000
		SR-3029	9.64	0.81	0.254
		PF-5006739	10.23	0.93	0.120
p38α	MAPK14	SB-239063	10.32	0.91	0.022
		SB-203580	9.64	0.79	0.205
		BIRB-796	10.38	0.94	0.003
		SB-202190	10.39	0.86	0.000
		SB-706504	10.25	0.90	0.044
		TAK 715	7.50	0.37	0.370
CDK5	CDK5	(R)-roscovitine	8.45	0.86	0.603
		(R)-CR8	9.86	0.89	0.000
		Olomoucine	7.85	0.91	0.910
		Butyrolactone I	8.99	0.14	0.061
		Purvalanols A	9.13	0.90	0.327
		Hymenialdisine	9.69	0.85	0.072
ERK2	MAPK1	FR-180204	9.33	0.73	0.730
		AZD0364	12.02	0.97	0.000
		VX-11e	11.49	0.89	0.175
		Ravoxertinib	10.89	0.82	0.344
		Ulixertinib	10.81	0.88	0.396
GSK3β	GSK3B	A-1070722	8.10	0.48	0.414
		AZD 2858	10.35	0.95	0.365
		6BIO	8.58	0.60	0.457
		CHIR 98014	12.15	0.97	0.000
		Kenpaullone	7.46	0.58	0.580
		AR-A014418	8.50	0.81	0.630
		SB-216763	8.69	0.81	0.598
		SB-415286	8.87	0.70	0.490
		ARN25068	8.76	0.77	0.557
		ZDWX-25	8.64	0.66	0.494
		TC-G-24	7.85	0.61	0.559

KINASE	GENE	INHIBITORS	IC50-LIKE	BAL	SCORE
PKBβ	AKT2	CCT128930	10.11	0.83	0.196
		Afuresertib	10.09	0.86	0.208
		Capivasertib	9.68	0.74	0.268
		GSK690693	10.91	0.9	0.000
		Miransertib	7.52	0.23	0.230
		Ipatasertib	9.69	0.58	0.209
DYRK1A	DYRK1A	Harmine	10.19	0.93	0.333
		DYRK1-IN-1	8.97	0.78	0.780
		ZDWX-25	9.29	0.81	0.674
		T3 CLK	10.87	0.92	0.000
		INDY	9.42	0.86	0.656
		TC-S 7004	10.62	0.69	0.091
		TG 003	9.99	0.87	0.403
JNK3	MAPK10	SP600125	8.47	0.82	0.224
		AS601245	7.19	0.43	0.279
		JNK-IN-8	8.61	0.82	0.190
		Tanzisertib HCl	9.4	0.66	0.000
		JNK inhibitor IX	5.99	0.26	0.260
		Bentamapimod	8.21	0.44	0.154
CK2α	CSNK2A1	TBCA	7.7	0.64	0.640
		Silmitasertib (CX-4945)	11.15	0.91	0.111
		APL-5125	11.63	0.96	0.000
		BioE-1115	7.83	0.61	0.590

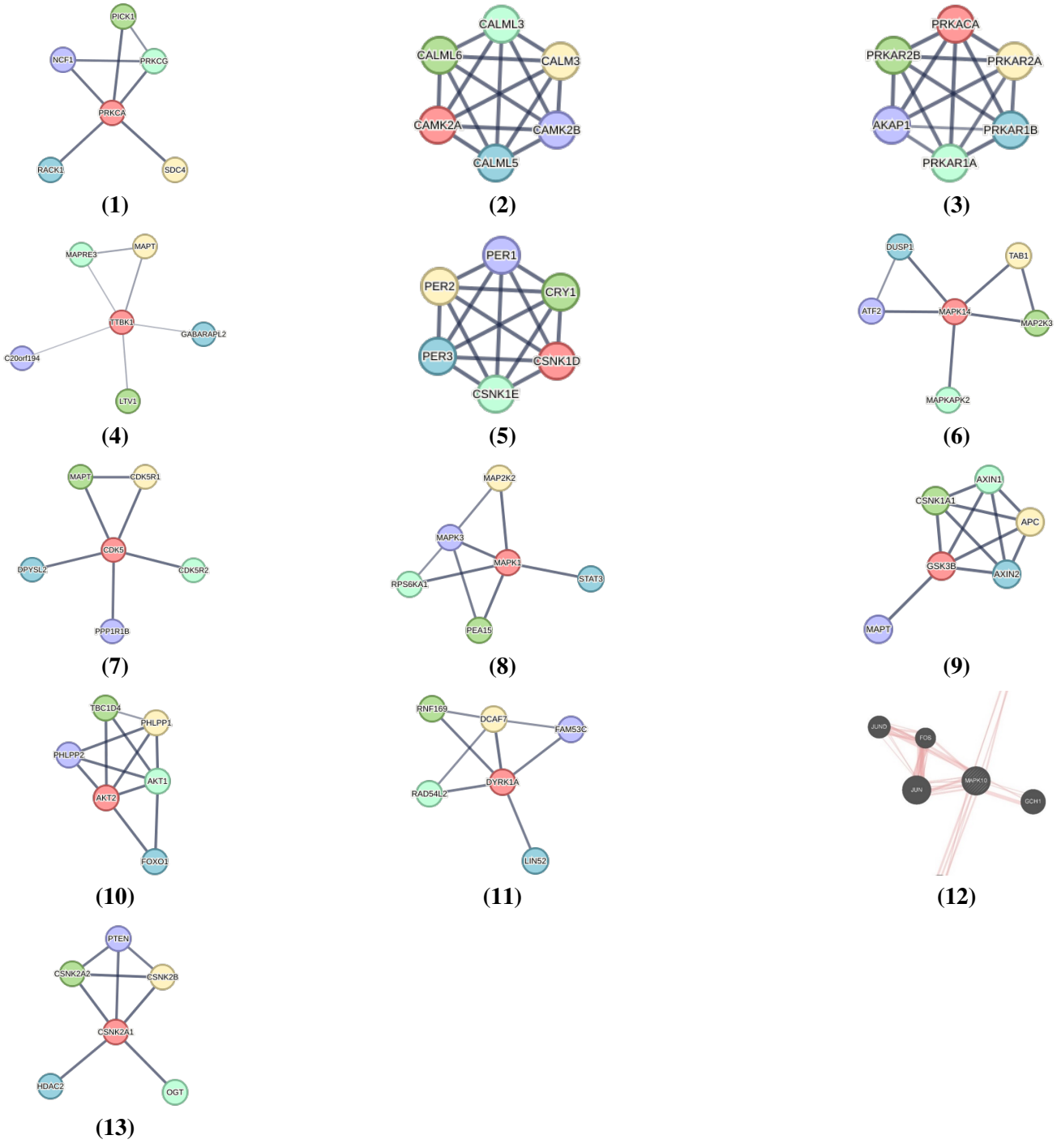

Figure S1 Illustration of the protein-protein interaction networks for all analyzed MAP tau kinases.